AIMS Mathematics, 10(12): 29552–29581.
DOI: 10.3934/math.20251298
Received: 18 September 2025
Revised: 22 November 2025
Accepted: 05 December 2025
Published: 15 December 2025

https://www.aimspress.com/journal/Math

Research article

Mechanical vibration response of CNT-reinforced nanocomposite conical shells using the Mori–Tanaka micromechanics model and FSDT

Saira Javed*

Department of Mathematics and Statistics, College of Science, King Faisal University, P.O. Box 400, Hofuf, Al Ahsa, 31982, Saudi Arabia

* **Correspondence:** Email: sulhaque@kfu.edu.sa.

Abstract: The free vibration behavior of carbon nanotube (CNT)-reinforced nanocomposite conical shells was investigated using the first-order shear deformation theory (FSDT) in conjunction with the Mori–Tanaka homogenization scheme. CNTs were incorporated into an epoxy matrix and E-glass fibers to enhance mechanical performance, particularly stiffness and damping characteristics. The effective material properties of the CNT-reinforced nanocomposite were computed using the Mori–Tanaka method, accounting for the volume fraction, orientation, and dispersion of CNTs within the matrix. A derivation of the dynamic equilibrium equations of motion for conical shells was carried out using Hamilton's principle, incorporating lateral shear deformation effects to improve accuracy for thick and moderately thick shells. An appropriate boundary condition associated with spline approximation was used to extract the natural frequencies. Ply orientation, number of layers, and shape parameters, including cone angle, length ratio, and circumferential node number, were considered to assess their influence on the frequencies. Numerical results demonstrate that matrix material significantly affects natural frequencies. Inclusion and exclusion of CNT in composites also alter the natural frequencies. These outcomes provide useful perspectives for improving the design and vibration mitigation of advanced nanocomposite conical shell structures used in aerospace, automotive, and marine engineering applications.

Keywords: carbon nanotube; reinforced nanocomposite; Mori–Tanaka model; matrix; frequency
Mathematics Subject Classification: 70H25, 74-10, 74A05, 74H15, 74H25, 74M20

1. Introduction

The Mori–Tanaka method is used for homogenizing composites with various types of reinforcements. Among them, carbon nanotubes (CNTs) are preferred for their exceptional stiffness and modulus. To analyze structural behaviors like free vibration, advanced modeling techniques are required to consider the scale-dependent and anisotropic nature of these materials.

Free vibration analysis helps to determine natural frequencies and mode shapes, critical for dynamic design and stability. The governing equations derived via FSDT are typically solved using different methods, such as Rayleigh–Ritz, Galerkin's, or the finite element method (FEM). These and other methods to solve such problems are used in the studies mentioned below.

Afshari and Amirabadi [1] studied the shuddering of cone-shaped structures reinforced with CNTs, in which material properties were derived via the Eshelby–Mori–Tanaka approach, vibrational behavior was modeled using FSDT, and natural frequencies were calculated via the generalized differential quadrature (GDQ) method. CNT agglomeration was shown to significantly decrease natural frequencies, while higher agglomeration levels lead to more pronounced stiffness degradation. This work extended classical FSDT by including realistic dispersion effects. Validation was limited to prior numerical data, instead of experimental benchmarks. In addition to this, a lack of exploration of graded or rotating shells makes generalization to FG-CNT or rotating configurations limited. Moreover, the study did not examine functionally graded CNT distributions, hybrid reinforcement patterns, or advanced CNT orientation strategies, restricting the generality of the conclusions to uniformly dispersed CNT composites. Rotating or spinning configurations, which are highly relevant to aerospace and rotor applications, were also not considered, reducing the applicability of the findings to dynamic environments involving centrifugal or Coriolis effects. Finally, the analysis remains within linear vibration assumptions, without exploring geometric nonlinearities, thermal influences, or viscoelasticity, all of which can significantly alter vibration characteristics in real-world operating conditions. Present research fills a scientific gap by using the spline approximation technique in analyzing the vibration behavior of CNT-reinforced nanocomposite conical shells.

Alinejad et al. [2] used the FSDT displacement model to examine the natural frequency of tapered shells with CNT-reinforced FG porous face layers and magnetorheological elastomer. The solution was based on semi-analytical methods (triangular functions circumferentially and DQM meridionally). Moreover, the Mori–Tanaka model was used for the FG-CNT face layers. Findings showed that face-layer porosity and CNT grading significantly influence both frequencies and damping (loss factors). In addition, end conditions strongly affect dynamic responses, especially in FG configurations. This study provided a novel combination of FG-CNT, porous layers, and a smart MRE core. Analysis was limited to linear vibration and focused more on forced/damped scenarios rather than pure free vibration. Buckling response or rotational dynamics were not addressed in this study.

Bina et al. [3] analyzed wavy CNT-enhanced face sheets on a sandwich cylindrical and conical shell. 3D elasticity theory was used with the generalized DQ method. This method extended micromechanics beyond Mori–Tanaka to include waviness and tube–tube contact. The findings of this study show that waviness and damaged core presence significantly lower natural frequencies. Moreover, the 3D elasticity model yields lower frequency predictions compared to FSDT models. Although the study focused on cylindrical shells, it offers direct implications for conical geometries. It demonstrates limitations of Mori–Tanaka homogenization when CNT morphology is non-ideal and provides high computational complexity compared to FSDT methods. Furthermore, the study does not

include experimental validation or comparison with multiscale finite element models, leaving uncertainty regarding the real-world accuracy of the predicted reductions in natural frequencies caused by CNT waviness and core damage. Finally, the investigation remains within the framework of linear vibration analysis; thermal loading, nonlinear deformation, environmental effects, and viscoelasticity factors known to strongly influence nanocomposite shell behavior were not explored. The current study fills such a gap by using FSDT to reduce computational complexity.

Afshari and Amirabadi [1] and Bina et al. [3] applied MT for CNT fractions of up to 5%–8% and reported acceptable accuracy when dispersion is assumed to be ideal. In our work, the 5% CNT volume fraction is selected only as an upper-bound design case; the primary trends remain consistent across lower fractions. Nevertheless, we now clearly acknowledge MT's limitations at higher CNT contents and include this point in both the discussion and the limitations sections.

Arshadi et al. [4] applied FSDT to sandwich shells with FG-CNT face sheets and auxetic honeycomb cores, including ring stiffeners. The problem was solved analytically and semi-analytically. Findings of the study show that the auxetic core combined with CNT-reinforced face sheets significantly boosts dynamic stiffness and alters the frequency spectrum. This study combines advanced core architecture (auxetic honeycomb) with CNT reinforcement in a conical shell context. Moreover, the study focused on sandwich/face-core interaction rather than standalone solid CNT-reinforced conical shells. The Mori–Tanaka method was used peripherally for CNT modeling, and the analysis remained limited to linear vibration behavior. Nonlinear dynamic effects, thermal gradients, viscoelastic core response, and geometric imperfections, which are critical in real aerospace and mechanical applications, were not included. The study also lacked experimental validation or comparison with multiscale finite element models, leaving uncertainty regarding the practical accuracy of the predicted improvements in stiffness and frequency response. Finally, although both analytical and semi-analytical approaches were employed, the semi-analytical method still relies on simplifying assumptions that may restrict its applicability to more complex boundary conditions, non-uniform CNT patterns, or irregular shell geometries.

Mallek et al. [5] studied a 3D FSDT finite-element model incorporating CNT agglomeration via a statistical agglomeration parameter. This study demonstrated that CNT clustering significantly reduces both stiffness and natural frequencies by up to 15% lower than perfectly dispersed cases. The author was the first to couple through-thickness stretch with agglomeration in a 3D FSDT framework. This was an extensive parametric study on agglomeration level, volume fraction, and boundary conditions; however, its limitation was that it relied on a single agglomeration parameter, while real CNT networks may exhibit more complex clustering behavior. Moreover, it neglected geometric nonlinearities and damping, which can be important at higher modes or large amplitudes.

Cho et al. [6] investigated FSDT displacement field mapped onto a 2D planar natural element method (NEM) mesh with Mori–Tanaka to obtain a graded elastic modulus. The NEM approach achieved <5% error against benchmark solutions, even on coarse grids, and identified that grading patterns (e.g., top-heavy vs. bottom-heavy CNT distribution) can tune mode shapes more effectively than uniform distribution. The mesh-free nature allows for complex shell geometries without remeshing. Rigorous validation was conducted against both Donnell's theory and FSDT finite elements. The limitation of this study was that planar mapping overlooked curvature in the element stiffness matrix, which may introduce small geometric errors for steep cone angles. Moreover, only linear free vibration was studied, and there was no treatment of thermal or rotational effects.

Amirabadi et al. [7] studied FSDT with centrifugal and Coriolis accelerations included for rotation. The Mori–Tanaka model was used for effective moduli, paired with a power-law gradation in both thickness and volume fraction. Non-uniform thickness (thicker at small radius) can increase first-mode frequency by ~8%, counter-intuitively stiffening the shell edge against rotation. Functionally graded volume fraction (higher at mid-span) counters rotational softening. The strength of this study was that it integrated rotation**,** graded thickness, and graded CNT content in one model and highlighted design levers for aerospace turbine casings. The limitation was that it used a constant shear correction factor, as accuracy deteriorates for very thick shells. Moreover, this study did not validate higher-order or 3D elasticity solutions.

The Halpin-Tsai, rule of mixtures, and Mori–Tanaka method are three micromechanical models. These models can estimate a composite's overall material behavior, especially composites reinforced with nanomaterials and, particularly, CNT-infused composites. Among them, the Mori–Tanaka homogenization method is the most accurate for inclusions in the matrix. This method handles random orientations, matrix-inclusion interaction, and nonlinearities, being more accurate for low filler volume fractions.

Studies like [8,9] effectively employed the Mori–Tanaka model to derive the homogenized elastic moduli of nanocomposite materials for use in continuum mechanics-based shell theories. This approach is especially appropriate for moderately thick conical shells, where shear effects cannot be neglected. Xiang et al. [10] conducted a free dynamic analysis of functionally graded (FG) composites reinforced with CNT cone structures, comparing results from FSDT with higher-order shear deformation theories (HSDT), emphasizing the importance of shell thickness and tapering on dynamic response. Zhang and Liu [11] modeled laminated conical shells with CNT reinforcements using shear deformation theory and showed the significant effect of boundary conditions and geometric parameters on frequency. Thomas and Suresh [12] conducted parametric studies using FEM to verify semi-analytical FSDT solutions, highlighting the accuracy of the Mori–Tanaka model for low CNT volume fractions. Aghaei and Talebi [13] investigated uniform and functionally graded CNT distributions under thermal loading using Galerkin's method based on classical shell theory. Sofiyev et al. [14] focused on FG-CNT materials in conical shells under combined loading conditions using power-law grading. Heydarpour et al. [15] used Mori–Tanaka homogenization and FSDT for rotating FG-CNT cases for a number of boundary conditions. Ansari et al. [16] examined free vibration and stability under axial loads with Mori–Tanaka-based FG-CNT models for functionally graded CNT-reinforced composite structures. Kiani et al. [17] used a detailed FSDT model for FG-CNT conical panels, validated via differential quadrature methods. Tornabene et al. [18] applied FSDT for FG shell behavior and discussed graded CNTs in conical configurations. Bulut [19] conducted FEA-based vibration studies of composite conical shells with different fiber orientations, complementing CNT-reinforced investigations.

Shadmani et al. [20] derived nonlinear motion equations via FSDT with von Kármán strains and solved them using Galerkin and Poincaré–Lindstedt methods for periodic amplitude-dependent frequencies. While not CNT-specific, this demonstrates the application of FSDT in a nonlinear dynamic setting for conical shells. The nonlinear regime analysis of graded shells sets a useful benchmark for future CNT-shell studies. However, this study lacked CNT reinforcement modeling, so Mori–Tanaka homogenization and CNT effects are absent.

Shi et al. [21] examined a state space, piecewise, analytical, and semi-analytical solution for free vibration of assembled spherical conical shell systems. A rigorous state space formulation and

piecewise matching provided high accuracy for multi-segment shell assemblies, which is useful as a benchmark for complex geometries. It focuses on a geometrical solution methodology rather than on advanced material microstructure, with no nanofiller homogenization or CNT-specific micromechanics. Applying this framework to CNT-reinforced shells would require coupling their mechanical formulation with a micromechanics homogenization step.

Shi et al. [22] developed a traveling wave solution and precise integration transfer matrices for spinning, thick multi-conical shells. This study addressed rotation and spinning (important for rotors in aircraft) with careful transfer matrix accuracy, valuable where Coriolis centrifugal effects are non-negligible. Material modeling remains classical. It also did not treat nanocomposite homogenization details (CNT waviness or interphase), so it does not resolve micromechanical uncertainties. The present study fills this gap. Zhang et al. [23] investigated the free vibration of FG metal foam panels reinforced with graphene platelets using the Halpin–Tsai extended rule of mixtures for effective properties, considering a solid treatment of porous metal foam graphene platelets, a clear exposition of homogenization choices, and sensitivity to porosity dispersion. Effects such as agglomeration, nonlinearities, and interface degradation were not considered.

Bayat et al. [24] conducted a comprehensive review of structural behavior and computational methods for CNT-reinforced structural elements. It provides a detailed up-to-date synthesis of modeling choices such as micromechanics approaches, classical vs. refined plate shell theories, and treatments of agglomeration waviness. Kiarasi et al. [25] conducted a dynamic transient impulsive analysis of the FG-CNTRC beam on a viscoelastic foundation using higher-order beam theory. Nonetheless, such analysis was confined to one-dimensional beam structures and did not extend to shell geometries. The present study fills this gap. Additionally, nonlinear effects, temperature-dependent material properties, and CNT imperfections were not incorporated.

Khatoonabadi et al. [26] focused on the buckling of porosity of graphene platelets using Halpin–Tsai effective properties. A thorough parametric study for porosity distribution demonstrated the sensitivity of stability results to microstructural grading. Although the porosity distribution was thoroughly examined, the work made simplifying assumptions regarding perfect GPL dispersion and did not explore nonlinear buckling or post-buckling behavior. The influence of GPL orientation or interphase effects is also absent. Babaei et al. [27] studied torsional buckling of FG porous truncated conical shell panels with GPL reinforcement and examined GPL patterns, porosity, and foundation effects. While a rich parametric study was conducted, the analysis was restricted to torsional loading and did not evaluate combined or complex loading states, such as shear deformation. The present study fills this gap. The modeling assumed ideal porosity distributions and perfect graphene platelet behavior.

Bayat et al. [28] investigated the natural frequencies of stiffened FG graphene-reinforced multilayer plates on elastic foundations, conducting a broad, parametric study. Parametric mapping of stiffeners, cutouts, and foundation stiffness was carried out, helping to understand how structural features dominate modal behavior. The study did not incorporate nanoscale effects such as CNTs, temperature dependence, or nonlinearity. Experimental correlation was also lacking. Hemmatnezhad et al. [29] demonstrated how geometric imperfections induce modal localization and alter modal ordering in cylindrical shells. The study highlighted an important practical effect (imperfections) that significantly modifies modal localization and must be considered in comparisons with idealized models. It also highlighted critical, practical issues, yet focused solely on specific imperfection patterns and did not examine multiscale reinforcement. The present study fills this gap, including thermal effects or nonlinear material behavior that may interact with imperfections.

Zippo et al. [30] conducted experimental and numerical studies on nonlinear shell dynamics under thermal gradients, showing strong thermal influence on nonlinear response and resonance phenomena. The study combined experiments and nonlinear theory to provide authoritative evidence that thermal gradients and nonlinearities fundamentally change shell dynamics. Although authoritative, the investigation was limited to conventional materials and did not incorporate nanocomposites (as the present study does), graded reinforcements, or micromechanical modeling. The strong nonlinear thermal coupling observed was not extended to hybrid or multiscale shell systems. Amabili [31] conducted a comprehensive monograph on geometrically nonlinear vibrations, compared the theory with experimental results, provided model comparisons, and used reduced-order techniques. The study presented an authoritative treatment of nonlinear shell behavior and a comparison among theories, regarded as essential background for anyone extending linear shell models to large amplitudes or thermal/nonlinear coupling. Soedel [32] is a classic reference covering linear vibration theory, practical examples, and complicating factors such as rotation and shear. Moreover, Leissa [33] is a classical NASA monograph providing fundamental solutions and benchmarks for shell vibration, with both thin shell theory and canonical geometries. The study provided a timeless benchmark for modal frequencies and mode shapes that are often used to validate new numerical and analytical formulations.

Amabili [34] did a comparative study of different shell theories, such as Donnell, Sanders, and Flügge, for large-amplitude vibrations. It demonstrated which theories are appropriate depending on amplitude and accuracy requirements, which is very relevant to model selection.

Recent research (2024 and 2025) in [7,24] has deepened modeling accuracy by incorporating CNT agglomeration, functionally graded CNT distributions, and advanced substrates like porous or smart core shells. However, most FSDT-based studies remain limited to linear free vibration, static thermal effects, and simplified shell geometries**.** The 3D elasticity-based studies expose the over-predictions of FSDT/Mori–Tanaka models when CNT morphology is non-ideal or when core defects exist. Yet, comprehensive models combining grading, rotation, nonlinearity, and thermal effects for conical shells are still notably missing.

Several parameters influence the CNT-reinforced conical shell's vibrational features:

- CNT volume fraction V_f : Higher V_f enhances stiffness, thus increasing natural frequencies.
- Geometry (cone half angle, ratio of material's thickness to its radius): Affects mode shapes and critical frequencies.
- Boundary conditions: Clamped and simply supported ends drastically alter the dynamic response.
- CNT distribution: Uniform vs. functionally graded distribution significantly alters the stiffness profile along the thickness.

The influence of the above-mentioned factors on the shuddering of CNT-reinforced cone-shaped structures is evident from the outcomes of the current study.

A number of studies used FSDT and the Mori–Tanaka model for CNT-reinforced conical shells. For example, in [1], the authors used the differential quadrature method; the natural element method was used in [6]; the differential quadrature method was used in [7]; the Ritz method was used in [10]; and the differential quadrature method was used in [15] for numerical computation. As such, the distinct novelty of this work that has not yet been covered is the spline approximation technique. This research is based on the vibrational behavior of CNT-reinforced nanocomposite conical shells using the FSDT in conjunction with the Mori–Tanaka homogenization scheme. FSDT (Mindlin Reissner

theory) improves upon the classical laminate plate theory (CLPT) by including transverse shear deformation, allowing for a linear variation of displacement across the thickness and introducing shear correction factors. For material modeling, the Mori–Tanaka homogenization method is used for estimating the effective mechanical properties of CNT-reinforced composites. It accounts for:

- The volume proportion of CNTs (V_f).
- Orientation and distribution, which are aligned in this study.
- Efficiency factors for transverse and shear load transfer (ξ and η).

In this study, aligned CNTs are embedded within an epoxy matrix and E-glass fibers to enhance mechanical properties, especially stiffness and damping. The macroscopic material properties are calculated using the Mori–Tanaka method, considering CNT volume fraction, alignment, and dispersion within the matrix and fibers. The dynamic equilibrium equations for the cone-shaped shell are formulated using Hamilton's principle, incorporating lateral shear deformation to improve accuracy, particularly for thick and moderately thick shells. The effects of end conditions, ply orientations, ply number, and structural geometry characteristics such as cone angle, length-to-radius ratio, and circumferential node number are investigated for their influence on natural frequencies. Numerical analysis shows that the choice of matrix and fibers plays a decisive effect in determining vibration characteristics. The presence or absence of CNTs in the composite also leads to notable changes in natural frequencies. The parameters with the largest influence in composite shells is the thickness ratio γ and CNT effective stiffness (CNT volume + dispersion + orientation). Geometry (cone angle and length ratio) is also strong, but its effect is mode dependent. CNTs change the effective elastic moduli and density of the composite shell. The Mori–Tanaka homogenization method provides the effective Young's modulus, shear, and bulk moduli used in FSDT. Higher effective stiffness (for the same mass distribution), in return, produces higher natural frequencies. The volume fraction (V_f) is related to effective stiffness, so it definitely affects frequencies. Aligned CNT orientation is more effective at increasing directional stiffness (longitudinal modulus).

Limitations of the study

1) The Mori–Tanaka method assumes dilute, well-dispersed inclusions and uses average-field interactions; it can under- or overestimate effective properties when the CNT volume fraction is high, CNTs agglomerate, or interactions are strong.
2) The perfect-dispersion assumption may overestimate the effective moduli and natural frequencies**.**
3) The classical Mori–Tanaka (MT) homogenization scheme provides the most accurate predictions at low CNT volume fractions due to its assumption of dilute and uniformly dispersed inclusions. Specifically, previous studies (e.g., Afshari & Amirabadi [1]; Bina et al. [3]) have applied MT for CNT fractions up to 5%–8% and reported acceptable accuracy when dispersion is assumed to be ideal. In our work, the 5% CNT volume fraction is selected only as an upper-bound design case; the primary trends remain consistent across lower fractions. Although idealized, this assumption aligns with the standard Mori–Tanaka homogenization approach, which requires geometrically simple, ellipsoidal inclusions. More advanced micromechanics models capable of incorporating waviness (e.g., "wavy CNT" models, orientation distribution–based MT variants) fall outside the scope of the present analytical study.
4) Aligned CNTs may not capture the frequency shifts introduced by random orientation, especially in torsional and coupled modes.

5) The model typically assumes uniform distribution and a prescribed orientation (e.g., aligned, random). Real composites often show non-uniform dispersion and local alignment variations that affect stiffness and vibration.
6) CNTs are often wavy or curved in actual materials; treating them as straight inclusions inflates predicted stiffness and natural frequencies.
7) Homogenization treats the interface implicitly (perfect bonding). Interfacial sliding, debonding, or imperfect load transfer (especially at high strain or under fatigue) are not captured.
8) FSDT + classical continuum homogenization ignores nonlocal elasticity/surface energy effects that can be important for very thin shells or very small CNT-reinforced layers.
9) FSDT assumes a linear transverse shear strain distribution and requires a shear correction factor; for very thick shells or strong through-thickness property gradients, higher-order theories might be more accurate.
10) Using a single shear correction factor, e.g., 5/6 for all layups and thicknesses, is an approximation; its best value depends on geometry and material through thickness variation.
11) The adopted shear correction factor follows the classical FSDT formulation commonly employed in conical shell analyses and is consistent with values used in recent studies on CNT-reinforced shells. To improve transparency, advanced formulations require additional kinematic assumptions outside the scope of the present analytical model; the classical approach was adopted for consistency with comparable literature.
12) The analysis assumes linear vibrations. Geometric nonlinearity (large deflections) and material nonlinearity (plasticity, damage) are not considered and can change frequencies and mode shapes under large amplitudes.
13) The study neglects structural damping, viscoelasticity, or energy dissipation mechanisms so it predicts undamped natural frequencies only.
14) A perfectly, simply supported boundary is assumed, whereas real supports are often elastic or imperfect and can shift frequencies and mode shapes.
15) Thermal stresses, temperature-dependent material properties, moisture, or chemical aging were not considered, but can significantly affect stiffness and vibration.
16) Material property scatter (CNT properties, matrix properties, interphase properties) and model sensitivity to those uncertainties are not quantified.

2. Mechanics-based formulation

The dynamic equilibrium equations for conical shells are as follows:

$$\begin{aligned}
&N_{x,x}+\tfrac{1}{x}(N_x-N_\theta)+\tfrac{1}{x\sin\alpha}N_{\theta x,\theta}=I_1u_{0,tt},\\
&N_{x\theta,x}+\tfrac{2}{x}N_{x\theta}+\tfrac{1}{x\sin\alpha}N_{\theta,\theta}+\tfrac{1}{x\tan\alpha}Q_{\theta z}=I_1v_{0,tt},\\
&Q_{xz,x}+\frac{1}{x}Q_{xz}+\frac{1}{x\sin\alpha}Q_{\theta z,\theta}-\frac{1}{x\tan\alpha}N_\theta=I_1w_{0,tt},\\
&M_{x,x}+\frac{1}{x}\left(M_x-M_\theta\right)+\frac{1}{x\sin\alpha}M_{\theta x,\theta}-Q_{xz}=I_3\psi_{x,tt},
\end{aligned} \tag{1}$$

$$M_{x\theta,x}+\frac{2}{x}M_{x\theta}+\frac{1}{x\sin\alpha}M_{\theta,\theta}-Q_{\theta z}=I_3\psi_{\theta,tt},$$

where $N_x, N_\theta, N_{x\theta}$ are the stress resultants in the respective directions, $M_x, M_\theta, M_{x\theta}$ are the bending and twisting moment resultants in corresponding orientations, and $Q_{xz}, Q_{\theta z}$ are the lateral shear resultants in the corresponding orientations.

The strain displacement relations are

$$\kappa_x=\psi_{x,x},\ \kappa_\theta=\frac{1}{x\sin\alpha}\psi_{\theta,\theta}+\frac{1}{x}\psi_x,\ \kappa_{x\theta}=\frac{1}{x\sin\alpha}\psi_{x,\theta}+\psi_{\theta,x}-\frac{1}{x}\psi_\theta,$$

$$\varepsilon_x=u_{0,x}+z\psi_{x,x},\ \varepsilon_\theta=\frac{1}{x}u_0+\frac{1}{x\sin\alpha}v_{0,\theta}+\frac{1}{x\tan\alpha}w+z\left(\frac{1}{x\sin\alpha}\psi_{\theta,\theta}+\frac{1}{x}\psi_x\right), \tag{2}$$

$$\gamma_{x\theta}=\frac{1}{x\sin\alpha}u_{0,\theta}+v_{0,x}-\frac{1}{x}v_0+z\left(\frac{1}{x\sin\alpha}\psi_{x,\theta}+\psi_{\theta,x}-\frac{1}{x}\psi_\theta\right),$$

$$\gamma_{\theta z}=\frac{1}{x\sin\alpha}w_{,\theta}-\frac{1}{x\tan\alpha}v_0+\psi_\theta,\ \gamma_{xz}=\psi_x+w,x,$$

where $\varepsilon_x, \varepsilon_\theta$ are the strain components in the axial direction, $\gamma_{x\theta}, \gamma_{xz}, \gamma_{\theta z}$ are the strain components in the shear direction, and $\kappa_x, \kappa_\theta, \kappa_{x\theta}$ are the deformation-induced curvatures of the midplane deformation for the corresponding orientations for the conical shell.

The displacement components are

$$u(x,\theta,z,t)=u_0(x,\theta,t)+z\psi_x(x,\theta,t),$$

$$v(x,\theta,z,t)=v_0(x,\theta,t)+z\psi_\theta(x,\theta,t), \tag{3}$$

$$w(x,\theta,z,t)=w(x,\theta,t),$$

where u, v, and w are the supplanting functions in x, θ, and z -corresponding orientations, u_0, v_0, and w are the spatial deviation of the mid plane of the cone, and ψ_x, ψ_θ are the rotational deformations of the cone's neutral axis due to shear forces. The material properties used via Mori–Tanaka methods are as follows:

Longitudinal Young's modulus (along the CNT axis):

$$E_{11}=E_m.\left[\frac{(1-V_f)+V_f.\frac{E_{CNT}}{E_m}}{1}\right]$$

Transverse Young's modulus (perpendicular to CNT axis):

$$E_{22} = E_m \cdot \left[\frac{1 + V_f \cdot \dfrac{E_{CNT,t} - E_m}{E_m + \xi(E_{CNT,t} - E_m)}}{1 - V_f} \right]$$

E_{CNT} : Young's modulus of CNT

E_m : Young's modulus of matrix

ξ : Shape-dependent factor

V_f : CNT volume fraction

Longitudinal shear modulus:

$$G_{12} = G_m \cdot \left[\frac{1 + V_f \cdot \dfrac{G_{CNT} - G_m}{G_m + \eta(G_{CNT} - G_m)}}{1 - V_f} \right]$$

Transverse shear modulus:

$$G_{23} = G_m \cdot \left[\frac{1 + V_f \cdot \dfrac{G_{CNT} - G_m}{G_m + \eta(G_{CNT} - G_m)}}{1 - V_f} \right] \tag{4}$$

G_{CNT} : Shear modulus of CNT

G_m : Shear modulus of matrix

η : Shape-dependent factor

V_f : CNT volume fraction

The dynamic equilibrium equations characterizing the shuddering of a conical shell, including FSDT, are as follows:

$$\left(A_{11} \frac{\partial^2}{\partial x^2} + \frac{1}{x} A_{11} \frac{\partial}{\partial x} + A_{66} \frac{1}{x^2 \sin^2 \alpha} \frac{\partial^2}{\partial \theta^2} - A_{22} \frac{1}{x^2} \right) u +$$

$$+ \left(\left(A_{12} + A_{66} \right) \frac{1}{x \sin \alpha} \frac{\partial^2}{\partial x \partial \theta} - \left(A_{22} + A_{66} \right) \frac{1}{x^2 \sin \alpha} \frac{\partial}{\partial \theta} \right) v$$

$$+ \left(A_{12} \frac{1}{x \tan \alpha} \frac{\partial}{\partial x} - A_{22} \frac{1}{x^2 \tan \alpha} \right) w = I_1 \frac{\partial^2 u}{\partial t^2}$$

$$\left(\left(A_{12} + A_{66} \right) \frac{1}{x \sin \alpha} \frac{\partial^2}{\partial x \partial \theta} + \left(A_{66} \frac{1}{x^2 \sin \alpha} + A_{22} \frac{1}{x^2 \sin \alpha} \right) \frac{\partial}{\partial \theta} \right) u$$

$$+\left(A_{66}\frac{\partial^2}{\partial x^2}+\frac{1}{x}A_{66}\frac{\partial}{\partial x}+A_{22}\frac{1}{x^2\sin^2\alpha}\frac{\partial^2}{\partial\theta^2}-A_{66}\frac{1}{x^2}+-KA_{44}\frac{1}{x^2\tan^2\alpha}\right)v$$

$$+\left(A_{22}+KA_{44}\right)\frac{1}{x^2\sin\alpha\tan\alpha}\frac{\partial w}{\partial\theta}+KA_{44}\frac{1}{x\tan\alpha}\psi_\theta=I_1\frac{\partial^2 v}{\partial t^2}$$

$$-\left(A_{12}\frac{1}{x\tan\alpha}\frac{\partial}{\partial x}+A_{22}\frac{1}{x^2\tan\alpha}\right)u-\left(A_{22}+KA_{44}\right)\frac{1}{x^2\sin\alpha\tan\alpha}\frac{\partial v}{\partial\theta}$$

$$+\left(KA_{55}\frac{\partial^2}{\partial x^2}+K\frac{1}{x}A_{55}\frac{\partial}{\partial x}+KA_{44}\frac{1}{x^2\sin^2\alpha}\frac{\partial^2}{\partial\theta^2}-A_{22}\frac{1}{x^2\tan^2\alpha}\right)w$$

$$\left(KA_{55}\frac{\partial}{\partial x}+K\frac{1}{x}A_{55}\right)\psi_x+KA_{44}\frac{1}{x\sin\alpha}\frac{\partial\psi_\theta}{\partial\theta}=I_1\frac{\partial^2 w}{\partial t^2}$$

$$-KA_{55}\frac{\partial w}{\partial x}+\left(D_{11}\frac{\partial^2}{\partial x^2}+\frac{1}{x}D_{11}\frac{\partial}{\partial x}+D_{66}\frac{1}{x^2\sin^2\alpha}\frac{\partial^2}{\partial\theta^2}+\right.$$

$$\left.-D_{22}\frac{1}{x^2}-KA_{55}\right)\psi_x+\left(\left(D_{12}+D_{66}\right)\frac{1}{x\sin\alpha}\frac{\partial^2}{\partial x\partial\theta}-\left(D_{22}\frac{1}{x}+D_{66}\frac{1}{x}\right)\frac{1}{x\sin\alpha}\frac{\partial}{\partial\theta}\right)\psi_\theta=I_3\frac{\partial^2\psi_x}{\partial t^2}$$

$$KA_{44}\frac{1}{x\tan\alpha}v-KA_{44}\frac{1}{x\sin\alpha}\frac{\partial w}{\partial\theta}+\left(\left(D_{66}+D_{12}\right)\frac{1}{x\sin\alpha}\frac{\partial^2}{\partial x\partial\theta}+\left(D_{66}\frac{1}{x}+D_{22}\frac{1}{x}\right)\frac{1}{x\sin\alpha}\frac{\partial}{\partial\theta}\right)\psi_x$$

$$+\left(D_{66}\frac{\partial^2}{\partial x^2}+\frac{1}{x}D_{66}\frac{\partial}{\partial x}++D_{22}\frac{1}{x^2\sin^2\alpha}\frac{\partial^2}{\partial\theta^2}-D_{66}\frac{1}{x^2}-KA_{44}\right)\psi_\theta=I_3\frac{\partial^2\psi_\theta}{\partial t^2}\tag{5}$$

The elastic coefficients A_{ij}, B_{ij}, and D_{ij} are the axial, coupling, and flexural rigidity stiffnesses, respectively [35].

The displacement components u, v, w and shear rotations ψ_x, ψ_θ are assumed in separable form, given as

$$u\ (x,\theta,t)=U(x)\cos n\theta\, e^{i\omega t},$$

$$v\ (x,\theta,t)=V(x)\sin n\theta\, e^{i\omega t},$$

$$w(x,\theta,t)=W(x)\cos n\theta\, e^{i\omega t},\tag{6}$$

$$\psi_x(x,\theta,t)=\Psi_x(x)\cos n\theta\, e^{i\omega t},$$

$$\psi_\theta(x,\theta,t)=\Psi_\theta(x)\sin n\theta\, e^{i\omega t},$$

where

ω = radian frequency of vibration
n = circumferential node number
t = time

The parameters used are:

$X = \dfrac{x-a}{l}$, $a \le x \le b$ and $X \in [0,1]$

$\lambda = \omega \ell \sqrt{\dfrac{I_1}{A_{11}}}$, a frequency variable

$\gamma = \dfrac{h_0}{r_a}$, ratios of the material's thickness to its radius of curvature

$\gamma' = \dfrac{h_0}{a}$, ratios of the material's thickness to its characteristic length

$\beta = \dfrac{a}{b}$, a length proportion

$\delta_k = \dfrac{h_k}{h}$, proportional layer width of the k-th layer.

Cubic spline functions are used to approximate the obtained differential equations, for $X \in [0,1]$. Supplanting functions $U(X)$, $V(X)$, $W(X)$ and rotating functions $\Psi_X(X)$, $\Psi_\theta(X)$ are approximated by cubic splines [36].

$$\begin{aligned}
U(X) &= \sum_{i=0}^{2} a_i X^i + \sum_{j=0}^{N-1} b_j (X - X_j)^3 H(X - X_j) \\
V(X) &= \sum_{i=0}^{2} c_i X^i + \sum_{j=0}^{N-1} d_j (X - X_j)^3 H(X - X_j) \\
W(X) &= \sum_{i=0}^{2} l_i X^i + \sum_{j=0}^{N-1} q_j (X - X_j)^3 H(X - X_j) \\
\Psi_p(X) &= \sum_{i=0}^{2} e_i X^i + \sum_{j=0}^{N-1} f_j (X - X_j)^3 H(X - X_j) \\
\Psi_q(X) &= \sum_{i=0}^{2} g_i X^i + \sum_{j=0}^{N-1} p_j (X - X_j)^3 H(X - X_j)
\end{aligned} \tag{7}$$

Here, $H(X - X_j)$ is the Heaviside step function, and N is the number of intervals into which the range $[0, 1]$ of X is divided. The points $X = X_s = \dfrac{s}{N}$, $(s = 0,1,2,.....,N)$, are chosen as the knots of the splines, as well as the collocation points. Thus, the splines are assumed to satisfy the differential equations given by Eq (7), at all X_s. The resulting expressions contain the $(5N+5)$ homogeneous system of equations in the $(5N+15)$ spline coefficients.

The boundary condition considered is as follows:

Simply-supported (S-S): both ends are simply supported:

$$V = W = \Psi_\theta = N_X = M_X = 0.$$

The simply supported end condition gives 10 more equations, thus making a total of $(5N+15)$ equations. The resulting equations are written as follows:

$$[\ O\ ]\{\ t\ \} = \lambda^2\ [\ P\ ]\ \{\ t\ \}, \tag{8}$$

where $[O]$ and $[P]$ are the $n \times n$ matrix, and $\{t\}$ is a column matrix. The generalized eigenvalue problem is the eigenfrequency parameter λ and the eigenvector $\{t\}$, whose components are the spline coefficients. The problem is solved to find the first three fundamental frequencies (eigenvalues) and their respective mode shapes (from eigenvectors). The equations are built from square matrices that include the material's stress, strain, and displacement, all of which determine the final frequency values.

3. Analysis and interpretation of results

In this study, the CNT-reinforced nanocomposite conical shells consisted of CNT/epoxy matrix and CNT/E-glass fibers composite materials with 5% CNT. Detailed material properties are given in Tables 1 and 2. Moreover, conical shells consisting of 3- and 5-layered Kevlar epoxy and E-glass epoxy composite materials were considered. The effect of CNT inclusion and exclusion on the frequency of shells was investigated by changing the length ratio, cone angle, and circumferential node number.

Table 1. Mechanical properties for both the epoxy matrix/CNTs and their effective composite using the Mori–Tanaka method (assuming aligned CNTs and 5% volume fraction).

Property	Symbol	Epoxy matrix	Carbon nanotubes (CNTs)	Composite (5% CNT)
Young's modulus (longitudinal)	E_{11}	3.5 GPa	1000 GPa	53.25 GPa
Young's modulus (transverse)	E_{22}	3.5 GPa	100 GPa	5.64 GPa
Longitudinal shear modulus	G_{12}	1.296 GPa	42 GPa	2.86 GPa
Transverse shear modulus	G_{23}	1.296 GPa	42 GPa	1.85 GPa
Poisson's ratio	ν_{12}	0.35	0.19	0.343
Density	ρ	1200 kg/m³	1600 kg/m³	1220 kg/m³
CNT volume fraction	V_f	-	-	0.05 (5%)
CNT transverse efficiency factor	ξ	-	-	2
CNT shear efficiency factor	η	-	-	2

Table 2. Mechanical properties for both the E-glass fibers/CNTs and their effective composite using the Mori–Tanaka method (assuming aligned CNTs and 5% volume fraction).

Property	Symbol	E-glass fibers	Carbon nanotubes (CNTs)	Composite (5% CNT)
Young's modulus (longitudinal)	E_{11}	76 GPa	1000 GPa	123.8 GPa
Young's modulus (transverse)	E_{22}	76 GPa	100 GPa	79.9 GPa
Longitudinal shear modulus	G_{12}	32 GPa	42 GPa	32.5 GPa
Transverse shear modulus	G_{23}	32 GPa	42 GPa	32.6 GPa
Poisson's ratio	ν_{12}	0.22	0.19	0.2185
Density	ρ	2550 kg/m³	1600 kg/m³	2483 kg/m³
CNT volume fraction	V_f	-	-	0.05 (5%)
CNT transverse efficiency factor	ξ	-	-	2
CNT shear efficiency factor	η	-	-	2

3.1. Convergence study

The frequency parameter with respect to different configurations was carried out to confirm the convergence of the spline method for conical shells. The number of subintervals N of the range $X \in [0,1]$ started at 4 and was fixed for N = 14, since for the next value of N, the percent changes in the λ values are very low, the maximum being 2%.

Table 3 shows a comparison of the reliability of the current results with those from the literature.

Table 3. Comparison of fundamental frequencies for the SS boundary condition.

R_0 / h	Xiang et al. [10]	Cho [6]	Present
25	7.1582	7.4946	7.3124
50	10.9383	10.8709	10.7312
100	16.6892	17.2480	17.1352

Another comparative analysis is shown in Table 4, which compares these results with those by Heydarpour et al. [15], Ansari et al. [37], and Tavakoli et al. [38]. It is clear that the outcomes from the current work are very close to those from existing literature.

Table 4. Comparison of the frequency value λ of the C-C CNT nanocomposite shells for different cone angles.

Cone angle	Heydarpour et al. [15]	Ansari et al. [37]	Tavakoli et al. [38]	Present
$\alpha = 15^0$	0.878	0.907	0.863	0.852
	0.642	0.657	0.637	0.626
$\alpha = 30^0$	0.822	0.824	0.819	0.805
	0.599	0.606	0.596	0.585

Table 5 shows the influence of CNT inclusion and exclusion on the frequency of 3- and 5-layered CNT-reinforced nanocomposite conical shells with respect to the length ratio. In both cases, the frequency value decreases with the increase in the number of layers. The nondimensional angular frequency ω is extremely sensitive to the length ratio β. In all cases, increasing β from 0.1 to 0.9 results in a massive frequency increase of over 1700%. The 5-layer Kevlar/epoxy shell shows the highest sensitivity. Adding CNTs to the epoxy matrix alone actually results in a slight decrease in frequency for this specific case (β = 0.5). However, using CNTs to reinforce the E-glass fibers leads to a dramatic increase in frequency, more than doubling it to over 100% increase. This demonstrates that placing CNTs in the fibers vs. the matrix is critical. Kevlar/epoxy shells consistently show a higher natural frequency than E-glass/epoxy shells, confirming that Kevlar provides a stiffer structure. The advantage is more pronounced in the 3-ply configuration. The effect of adding more layers (from 3 to 5) is not universal and depends on the base material. For Kevlar/epoxy, the 3-ply layup is stiffer. For E-glass/epoxy, the 5-ply symmetric layup is stiffer. This highlights the complex interactions between material properties and laminate stacking sequence.

Table 5. Influence of length ratio β on the nondimensional angular frequency ω of CNT-reinforced and CNT-free nanocomposite shells for various ply orientations and layups.

β	Exclusion of CNT				Inclusion of CNT			
	Kevlar epoxy		E-glass epoxy		CNT/epoxy matrix		CNT/E-glass fibers	
	$45^0/0^0/45^0$	$30^0/45^0/0^0/45^0/30^0$	$45^0/0^0/45^0$	$30^0/45^0/0^0/45^0/30^0$	$45^0/0^0/45^0$	$30^0/45^0/0^0/45^0/30^0$	$45^0/0^0/45^0$	$30^0/45^0/0^0/45^0/30^0$
0.1	219.051	198.595	144.595	164.138	206.23	196.075	300.09	300.88
0.3	655.661	599.115	466.282	496.856	624.47	589.612	1057.3	1052
0.5	1110.35	1030.38	779.143	849.524	1051.4	1004	1782.1	1774
0.7	1969.58	2099.02	1339.75	1768.2	1838.5	1950.52	3003.3	3038.43
0.9	4235.96	4232.89	2605.61	3072.17	3784.8	3779.82	5522.5	5522.35

Table 6 shows the influence of CNT inclusion and exclusion on the frequency of 3- and 5-layered CNT-reinforced nanocomposite conical shells with respect to cone angle. The nondimensional frequency is highly sensitive to the cone angle. In all cases, increasing the cone angle from 10° to 90° (i.e., making the shell more like a cylinder) results in a significant decrease in frequency, typically between 37% and 57%. The E-glass/epoxy shells show the greatest sensitivity to this change. The effect of CNT reinforcement is highly dependent on what it is reinforcing. Adding CNTs to the epoxy matrix results in a significant increase in frequency of around 18%. Conversely, adding CNTs to the E-glass fibers results in a large decrease in frequency of over 23%. This is a stark contrast to the previous table and suggests that the effect of CNT placement is complex and interacts with the cone angle and material properties. For conical shells at this angle, E-glass/epoxy shells have a significantly higher natural frequency over 42% than Kevlar/epoxy shells. This is the opposite of what was observed for the length ratio in Table 5, highlighting how the optimal material depends on the geometric parameters. For conical shells, the number of layers (3 vs. 5) has a very minor effect on the natural frequency, with differences of less than 2%. The 3-ply configuration is consistently slightly stiffer, but the effect is negligible compared to the influence of material and cone angle.

Table 6. Influence of cone angle α on the nondimensional frequency λ of CNT-reinforced and CNT-free nanocomposite shells for various ply orientations and layups.

α	Exclusion of CNT				Inclusion of CNT			
	Kevlar epoxy		E-glass epoxy		CNT/epoxy matrix		CNT/E-glass fibers	
	$45^0/0^0/45^0$	$30^0/45^0/0^0$ $/45^0/30^0$	$45^0/0^0/45^0$	$30^0/45^0/0^0/$ $45^0/30^0$	$45^0/0^0/45^0$	$30^0/45^0/0^0$ $/45^0/30^0$	$45^0/0^0/45^0$	$30^0/45^0/0^0$ $/45^0/30^0$
10	1.06923	1.00861	2.2206	2.2075	1.2551	1.1944	1.6899	1.42456
30	0.79769	0.81702	1.1965	1.1962	0.9074	0.9193	1.10495	1.09292
50	0.65633	0.64994	0.9332	0.9319	0.7412	0.7398	0.87918	0.86329
70	0.6205	0.61979	0.9434	0.9415	0.712	0.7138	0.89252	0.876619
90	0.61127	0.61217	0.9469	0.9447	0.7042	0.7069	0.90796	0.89427

Table 7 shows the influence of CNT inclusion and exclusion on the frequency of 3- and 5-layered CNT-reinforced nanocomposite conical shells with respect to circumferential node number. The inclusion of CNT increases the frequency of the shell. The nondimensional frequency is highly sensitive to the circumferential node number. In all cases, increasing n from 2 to 10 results in a very large increase in frequency, between 80% and 106%. This indicates that higher-order vibration modes with more waves around the circumference have significantly higher frequencies. The 3-ply Kevlar/epoxy shell shows the greatest sensitivity. Adding CNTs provides a consistent increase in natural frequency across all material systems for this vibration mode (n = 6). The most significant benefit is seen when CNTs are used to reinforce the E-glass fibers, with an increase of over 15% for the 3-ply and a substantial 30.1% for the 5-ply layup. Reinforcing the epoxy matrix also provides a clear benefit, increasing frequency by 7.5%–10.8%. For this specific mode (n = 6), E-glass/epoxy shells have a higher natural frequency than Kevlar/epoxy shells, with the 5-ply configuration showing a more pronounced advantage of almost 17%. This continues the trend observed with the cone angle, where E-glass outperforms Kevlar for this shell geometry. The effect of the number of layers is material-dependent. For Kevlar-based shells, the 3-ply layup is significantly stiffer (around 8%–9% higher frequency) than the 5-ply layup. For E-glass-based shells, the difference between 3 and 5 plies is very small (<1%), with the 3-ply being marginally stiffer.

Table 7. Influence of circumferential node number n on the nondimensional frequency λ of CNT-reinforced and CNT-free nanocomposite shells for various ply orientations and layups.

n	Exclusion of CNT				Inclusion of CNT			
	Kevlar epoxy		E-glass epoxy		CNT/epoxy matrix		CNT/E-glass fibers	
	$45^0/0^0/45^0$	$30^0/45^0/0^0$ $/45^0/30^0$	$45^0/0^0/45^0$	$30^0/45^0/0^0$ $/45^0/30^0$	$45^0/0^0/45^0$	$30^0/45^0/0^0$ $/45^0/30^0$	$45^0/0^0/45^0$	$30^0/45^0/0^0$ $/45^0/30^0$
2	0.3478	0.31587	0.42057	0.37002	0.3739	0.35	0.4862	0.4814
4	0.34061	0.32631	0.36378	0.3622	0.346	0.3351	0.3846	0.3826
6	0.37893	0.34475	0.40628	0.40297	0.3856	0.3547	0.4296	0.4232
8	0.52338	0.45105	0.57881	0.54623	0.5403	0.4747	0.6235	0.6096
10	0.7165	0.60188	0.81164	0.74053	0.7482	0.644	0.8852	0.8628

The influence of CNT-reinforced nanocomposites with different matrix materials on the frequency of conical shells with respect to circumferential node number is seen in Table 8. It shows that as the number of layers increases, the frequency also increases. Moreover, E-glass fibers show a higher frequency value compared to the epoxy matrix. Increasing the node number causes a large increase in frequency, from 70% to 95%. The 3-ply epoxy matrix system shows the highest sensitivity. The 5-ply layups for both materials show very similar sensitivity (~69%–79%).

Table 8. Influence of circumferential node number n on the frequency λ of CNT-reinforced nanocomposite with different materials for various ply orientation and layups.

n variation	Epoxy matrix		E-glass fibers	
	$30^0/0^0/30^0$	$30^0/60^0/0^0/60^0/30^0$	$30^0/0^0/30^0$	$30^0/60^0/0^0/60^0/30^0$
2	0.2734	0.4251	0.4563	0.4943
4	0.2689	0.3568	0.3635	0.3868
6	0.298	0.3802	0.4021	0.4307
8	0.3955	0.5237	0.5782	0.6235
10	0.5331	0.7207	0.8187	0.8842

The effect of CNT-reinforced nanocomposites with different matrix materials on the frequency of conical shells with respect to the length ratio is seen in Table 9. As the number of layers increases, the frequency value also increases. Moreover, E-glass fiber shows a significantly higher frequency value than the epoxy matrix. The length ratio is the most dominant parameter, causing astronomical increases in frequency (over 1700%). The 3-ply epoxy matrix system is the most sensitive. CNT/E-glass fibers consistently produce a much higher frequency than CNT/epoxy matrix across all parameters. The advantage is most pronounced for the length ratio and least pronounced for the 5-ply cone angle and node number. The effect of the layup is highly dependent on the base material. For the CNT/epoxy matrix, the 5-ply layup is significantly stiffer, increasing frequency by 20%–30%. For the CNT/E-glass fibers, the 5-ply layup provides only a marginal benefit from 2.7% to 7.1%, making the 3-ply layup nearly as effective for this material system.

Table 9. Influence of length ratio β on the nondimensional angular frequency ω of CNT-reinforced nanocomposite with different matrix and fibers for various ply orientations and layups.

β	Epoxy matrix		E-glass fibers	
	$30^0/0^0/30^0$	$30^0/60^0/0^0/60^0/30^0$	$30^0/0^0/30^0$	$30^0/60^0/0^0/60^0/30^0$
0.1	169.64	209.907	298.077	297.98
0.3	513.238	674.698	1031	1059.18
0.5	884.89	1145.77	1745.5	1792
0.7	1915.13	2032.52	3028.6	3038.81
0.9	3330	3795.49	5381.4	5524.4

The influence of CNT-reinforced nanocomposites with different matrix materials on the frequency of conical shells with respect to cone angle is seen in Table 10. Increasing the cone angle causes a strong decrease in frequency from 39% to 58%. E-glass fiber systems are more sensitive to

this change. The 5-ply layup is slightly more sensitive for the epoxy matrix, while the 3-ply is slightly more sensitive for the E-glass fibers.

The reason for the frequency decrease is not the increase in the number of layers itself, but the specific change in ply orientation that accompanied it. The 3-layer laminate (45/0/45) has a more optimal stacking sequence for maximizing bending stiffness (and thus natural frequency) than the 5-layer laminate (30/45/0/45/30) for this specific shell structure and boundary conditions. The effect of the less favorable orientation in the 5-layer laminate outweighs the benefit of having additional layers and a slightly greater overall thickness. It is concluded that stiffness is driven more by what the layers are made of (their orientation) and where they are placed, rather than just the raw number of layers.

Table 10. Influence of cone angle α on the nondimensional frequency λ of CNT-reinforced nanocomposites with different matrix and fibers for various ply orientations and layups.

α	Epoxy matrix		E-glass fibers	
	$30^0/0^0/30^0$	$30^0/60^0/0^0/60^0/30^0$	$30^0/0^0/30^0$	$30^0/60^0/0^0/60^0/30^0$
10	1.0743	1.3072	2.1232	2.2537
30	0.7954	0.9861	1.1322	1.201
50	0.6553	0.7859	0.8772	0.9383
70	0.6517	0.7561	0.8848	0.9482
90	0.6503	0.7472	0.8871	0.9515

Figure 1 shows the variation of radian frequency $\omega_m \times 10^3 Hz$ of 5-layered CNT-reinforced nanocomposite (CNT/epoxy matrix) conical shells with respect to the length proportion β with 5% CNT volume fraction. The factors are kept constant. It can be seen that the radian frequency variation between $\beta = 0.1$ and 0.6 is minimal, but then significant.

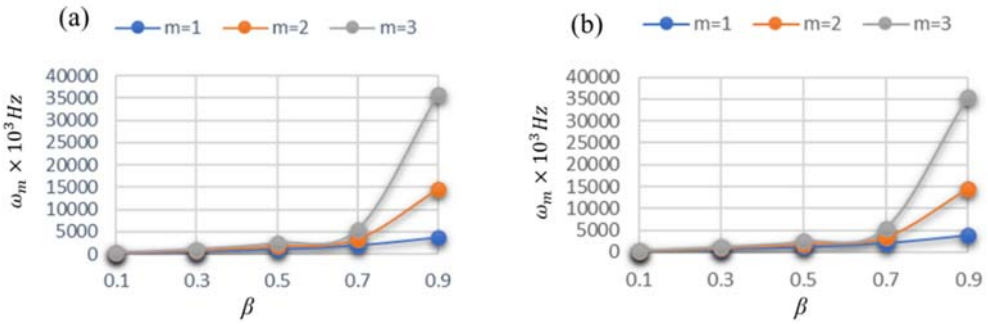

Figure 1. Radian frequency $\omega_m \times 10^3 Hz$ variation of CNT-reinforced nanocomposite (CNT/epoxy matrix) conical shells with respect to the length ratio β with 5% CNT volume fraction. The 5- layered ply alignment of the CNT-reinforced nanocomposite is (a) $30^0/45^0/0^0/45^0/30^0$, (b) $30^0/60^0/0^0/60^0/30^0$, $n = 2, \gamma = 0.05, \alpha = 45^0$.

Figure 1 reveals three distinct behaviors in the frequency vs. β relationship. For small and moderate length ratios $\beta(\beta \le 0.6)$, the first three modes exhibit a very weak dependence on β. This region corresponds to a shell that is relatively long compared to its characteristic radius, where the

deformation for the lower circumferential modes is governed primarily by membrane-dominated strain energy. The curves are almost flat in this region because the effective axial modulus E_{11} of the CNT-reinforced plies, derived from the Mori–Tanaka homogenization, is already high due to CNT stiffening. Thus, small changes in β do not significantly alter the extensional stiffness contribution. In this regime, geometric stiffening associated with conicity is minimal, and the shell behaves closer to a cylindrical structure. Moreover, all three modes are governed mostly by extensional membrane stiffness, and the difference between m = 1, 2, 3 remains relatively small. This region reflects weak geometric sensitivity and strong stiffness dominance.

As β increases beyond 0.6, the curves begin to separate, especially for modes m = 2 and m = 3. This marks the transition region where the local cone angle increases sufficiently, modifying the curvature distribution, the circumferential stretching stiffness, and shear energy contribution of FSDT terms with G_{12}. The key mechanism when β increases beyond 0.6 is as follows:

- Increasing β effectively shortens the shell while increasing the change in radius along the length, which enhances circumferential curvature.
- This curvature raises the modal stiffness for higher circumferential wave numbers (especially m = 3), making their frequencies more sensitive to geometric variation.
- The CNT reinforcement contributes more prominently to tangential extensional stiffness, amplifying differences between higher circumferential modes.

Thus, this region shows the interaction between CNT-induced stiffness and geometric curvature. The most striking feature is the sharp upward increase in frequency for all modes when β approaches 0.9, particularly for m = 3, which shoots up dramatically. This sharp increase corresponds to the geometric stiffening effect of the conical shell near the apex, where the radius decreases rapidly, membrane stiffness (proportional to radius and laminate extensional rigidity) increases sharply, and bending stiffness increases due to combined curvature effects. Because the CNT-reinforced plies significantly increase E_{11}, E_{22}, and, particularly , G_{12}, the stiffening effect becomes more pronounced in higher modes.

The mode m = 3 increases the most because it has more circumferential waves and higher curvature energy and is more sensitive to radial contraction. CNT stiffening substantially increases the shear modulus G_{12}, which strongly affects higher-order circumferential modes as predicted by FSDT. Near the small-radius end of the cone, the CNT-reinforced material behaves like a geometrically constrained membrane, pushing the frequency upward very sharply. Thus, the sharp rise reflects a combined CNT-material stiffening and geometric curvature amplification, with higher modes affected more strongly. Laminate sequences of $30^0/\ 45^0/0^0/\ 45^0/30^0$ emphasize in-plane extensional stiffness and moderate shear coupling, whereas $30^0/60^0/\ 0^0/60^0/30^0$ sequences introduce higher in-plane anisotropy and increased shear–extension coupling, making the shell slightly more sensitive to β near the conical apex. This explains why sequence (b) often yields slightly higher frequencies for m = 2 and m = 3, especially near $\beta = 0.9$. Overall, the figure highlights the interaction between CNT-induced material stiffening and geometry-driven curvature effects in governing the dynamic behavior of conical shells.

Figure 2 shows the frequency variation of 3- and 5-layer CNT-reinforced nanocomposite (CNT/epoxy matrix) conical shells with respect to the cone angle α . The factors $n = 2, \gamma' = 0.5, \beta = 0.5$ are kept constant. It is evident that the frequency value decreases as the cone angle increases. The decrease in the frequency value is significant until α =10–40 and is almost linear afterward. The plotted non-dimensional frequency measure λ_m for modes m = 1,2,3 drops

monotonically as α increases from 10° to 50° and then approaches a near constant value for α > 50°–70°. Physically, increasing the cone angle reduces the effective circumferential curvature seen by the shell for the same axial coordinate or, equivalently, changes how radius varies along the length, which changes the balance between the membrane and bending contributions to modal stiffness. For a large α, the geometry approaches a "flatter" cone segment or a geometry where additional increases in α produce diminishing changes in curvature distribution, so the dynamic stiffness saturates and λ_m levels off. The curves are ordered as $\lambda_m, m=3 > \lambda_m, m=2 > \lambda_m, m=1$ across α. This reflects that higher circumferential wave number modes store relatively more circumferential bending curvature energy and are therefore intrinsically stiffer (higher frequency) for the same overall stiffness field. The separation between modes is largest at small α and shrinks as α increases. At small cone angles, the structural curvature is pronounced, and small changes in α produce large changes in curvature distribution and therefore large changes in modal stiffness. That is why λ_m falls rapidly in this range; the shell's dynamics are curvature sensitive. At $\alpha \geq 50°$, the curvature and slope changes have a small incremental effect on the local stiffness distribution, so λ_m approaches an asymptotic value controlled primarily by material stiffness (CNT-enhanced moduli) and the laminate architecture rather than geometry. The two stacking sequences differ in directional stiffness and coupling. Sequences with more ±60° plies supply larger circumferential stiffness components and more shear extension coupling, increasing λ_m for higher m modes. The presence of a central 0° ply reduces anisotropic softening in the axial direction and helps maintain membrane stiffness as α varies. Therefore, the difference between 3- and 5-layer responses shows how ply architecture redistributes strain energy between circumferential extension, axial extension, and transverse shear changing mode sensitivities to α.

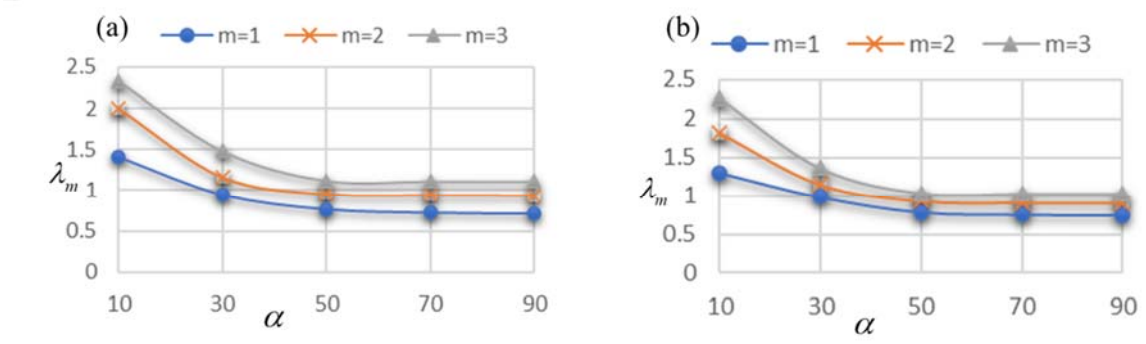

Figure 2. Frequency λ_m variation of CNT-reinforced nanocomposite (CNT/epoxy matrix) shells varies with the cone angle α with 5% CNT volume fraction. 3- and 5- layered ply alignment of CNT-reinforced nanocomposite is (a) $60^0/\ 0^0/60^0$, (b) $30^0/60^0/\ 0^0/60^0/30^0$, $n=2, \gamma'=0.5, \beta=0.5$

CNT reinforcement (Mori–Tanaka effective moduli) raises E_{11}, E_{22}, and G_{12}. Increased G_{12} makes FSDT shear terms more important for higher modes; increased E_{22} and E_{11} increase membrane stiffness. Because geometry determines how much of the modal energy is in bending vs. membrane vs. shear, the CNT effect couples with α to produce the observed α-dependent trend.

Increasing the cone angle changes the meridional curvature and meridional bending stiffness. A larger angle tends to reduce the effective meridional bending resistance and also changes the coupling

between bending and membrane strains, so the global stiffness of many vibrational modes falls and lowers the natural frequencies. For certain geometries, this also moves the lowest-frequency mode from one circumferential wave number to another.

- The effect is stronger for moderately thick shells where bending contributes significantly. For extremely thin shells, membrane effects dominate, and geometry-induced changes appear differently.
- If the design goal is to raise a particular natural frequency, decreasing the cone angle to make it more cylinder is typically beneficial.

Frequency λ_m variation of 3- and 5-layer CNT-reinforced nanocomposite (CNT/epoxy matrix) conical shells with respect to the circumferential node number n is seen in Figure 3. The factors $\beta = 0.5, \gamma = 0.05, \alpha = 45^0$ are kept constant. Frequency values first decrease and then gradually increase with the increase of circumferential node number.

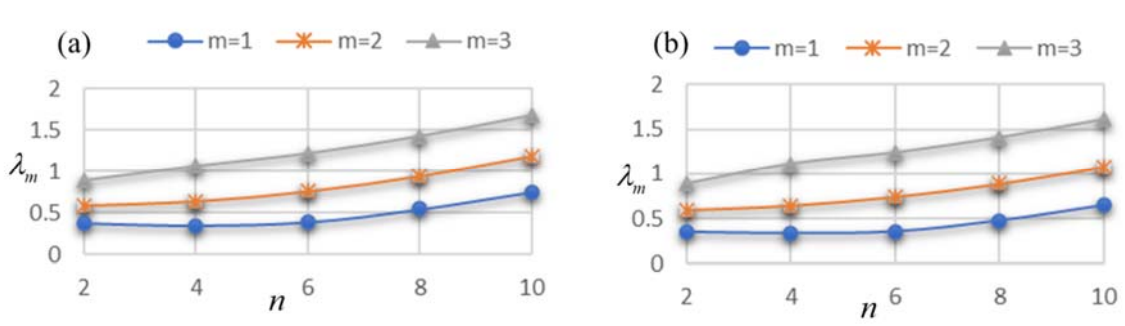

Figure 3. Frequency λ_m variation of CNT-reinforced nanocomposite (CNT/epoxy matrix) varies with the circumferential node number n with 5% CNT volume fraction. 3- and 5-layered ply alignment of CNT-reinforced nanocomposite is (a) $45^0/\ 0^0/45^0$, (b) $30^0/45^0/\ 0^0/45^0/30^0$, $\alpha = 45^0, \gamma = 0.05, \beta = 0.5$.

In both laminate configurations, the curves for all three values of m exhibit a monotonic increase in frequency as n increases. This behavior is physically expected since higher circumferential mode numbers correspond to shorter circumferential wavelengths, producing higher bending and shear stiffness and consequently higher vibration frequencies. The increase is smooth in both cases, indicating that CNT reinforcement stabilizes the dynamic response by enhancing stiffness uniformly throughout the laminate. The CNT reinforcement also contributes to this stiffening effect through enhanced E_{11}, E_{22}, and G_{12} predicted by the Mori–Tanaka model. The inclusion of 5% CNTs significantly alters the effective elastic properties, especially E_{11}, E_{22}, and G_{12}, due to strong CNT matrix interfacial load transfer. This enhancement is reflected in the upward shift of all frequency curves compared to conventional fiber-reinforced or pure epoxy shells. CNTs provide additional stiffness in the axial and circumferential directions, particularly benefiting higher order modes.

For both configurations (a) and (b), the curves are clearly ordered as $\lambda_m, m = 3 > \lambda_m, m = 2 > \lambda_m, m = 1$. The frequency separation between adjacent axial modes widens slightly with increasing n, indicating stronger coupling effects in higher circumferential modes. The presence of CNTs amplifies these separations because the stiffened matrix becomes more sensitive to mode shape curvature. This consistent ordering also indicates that the laminate configurations do not introduce modal crossover or

mode coupled instabilities. The $45^0/0^0/45^0$ configuration provides moderate axial stiffness (due to the central 0° ply) and high in-plane shear stiffness (due to the 45° plies). This configuration yields a balanced and symmetric stiffness profile. As reflected in the figure, the frequencies increase smoothly without abrupt slope changes, showing that the configuration is dynamically stable and mechanically efficient for moderate loading conditions. The $30^0/45^0/0^0/45^0/30^0$ configuration provides higher stiffness than the 3-layer laminate due to an increased number of plies. It provides more gradual stiffness transitions across thickness and better distribution of CNT-enhanced stiffness. The outer 30° layers add additional circumferential stiffness, while the inner 45° and 0° layers enhance shear and axial stiffness, respectively. As a result, the frequencies in Figure 3(b) are higher than those in Figure 3(a) for the same n and m, being more linear with respect to n, especially for higher modes, and less sensitive to CNT dispersion variability. This is because the 5-layer system distributes the CNT-induced stiffening more uniformly, minimizing localized deformation modes. Both figures depict shaded bands around each curve, representing uncertainty due to CNT agglomeration, nonuniform CNT distribution, modeling approximations, or variability in interfacial bonding. These bands widen slightly for large n, especially in configuration (a). This occurs because the 3-layer system experiences larger strain gradients in higher-order modes, making it more sensitive to uncertainty. The expected narrower bands in configuration (b) indicate better mechanical stability and more predictable vibration behavior due to the smoother distribution of stiffness.

Conical shells show non-monotonic curve frequency which may fall to the minimum at some end and then increase again. There are two broad mode families:

Inextensional (low n): Bending-dominated, large transverse motion offers lower frequencies for small n.

Regular/extension (low n): Membrane-dominated modes where in-plane stretching raises frequency scaling differently with geometry.

To avoid resonance, we have to do a full n sweep because small geometric tweaks can change which circumferential mode is the lowest and therefore which frequency you must avoid.

The effect of different matrices of CNT-reinforced nanocomposites on the radian frequency ω of conical shells with respect to the length proportion β is shown in Figure 4, with three different ply orientations.

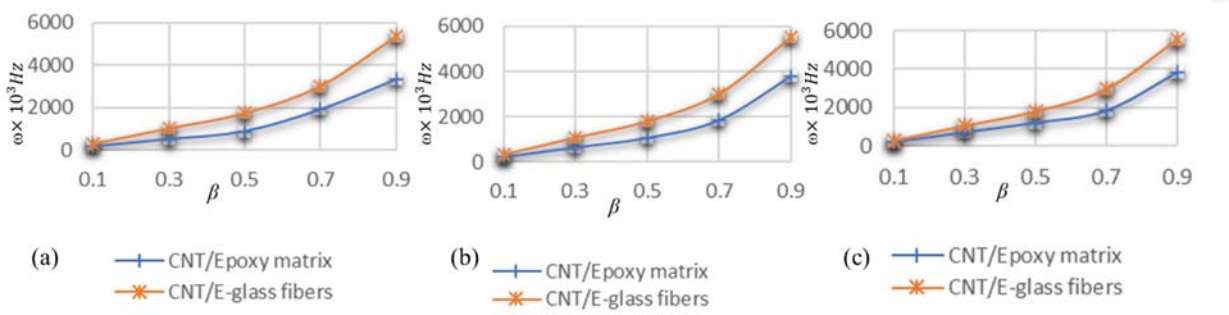

Figure 4. Radian frequency ω variation of CNT-reinforced nanocomposite conical shells with respect to the length ratio β with different matrix materials. 3- layered ply alignment of CNT-reinforced nanocomposite is (a) $30^0/0^0/30^0$, (b) $45^0/0^0/45^0$, (c) $60^0/0^0/60^0$.

The influence of different matrices of CNT-reinforced nanocomposites on the frequency of conical shells with respect to the cone angle is shown in Figure 5, with a 5-layer ply orientation. The

impact of different matrices of CNT on the frequency of conical shells with respect to the circumferential node number is shown in Figure 6, with a 5-layer ply orientation.

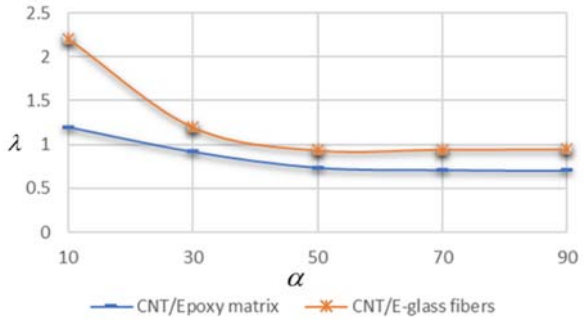

Figure 5. Frequency variation λ of CNT-reinforced nanocomposites varies with the cone angle α with different matrix materials. 5-layered ply alignment of CNT-reinforced nanocomposite is $30^0/45^0/\ 0^0/45^0/30^0$, $n=2, \gamma'=0.5, \beta=0.5$.

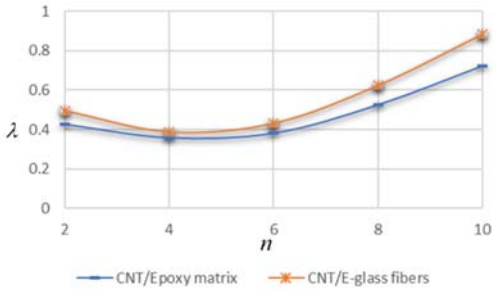

Figure 6. Frequency variation λ of 5-layered CNT-reinforced nanocomposite conical shells varies with the circumferential node number n for various matrix materials. Ply alignment of CNT-reinforced nanocomposite is $30^0/60^0/\ 0^0/60^0/30^0$, $\alpha=45^0, \gamma=0.05, \beta=0.5$.

Figure 7 depicts the frequency variation λ of 3-layered CNT-reinforced nanocomposite conical shells with respect to the circumferential node number n with different matrix materials.

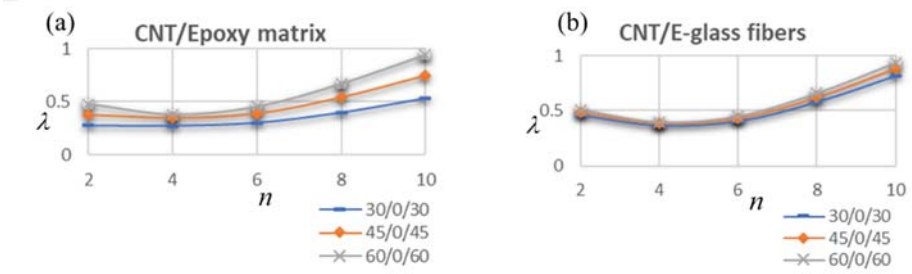

Figure 7. Frequency variation λ of 3-layered CNT-reinforced nanocomposite shells varies with the circumferential node number n under various matrix materials. $\alpha=45^0, \gamma=0.05, \beta=0.5$.

The effect of CNT inclusion and exclusion on the frequency of 3-layered CNT-reinforced nanocomposite conical shells with respect to the circumferential node number n is shown in Figure 8, while the same effect for 5-layered CNT-reinforced nanocomposite conical shells with respect to the cone angle is shown in Figure 9.

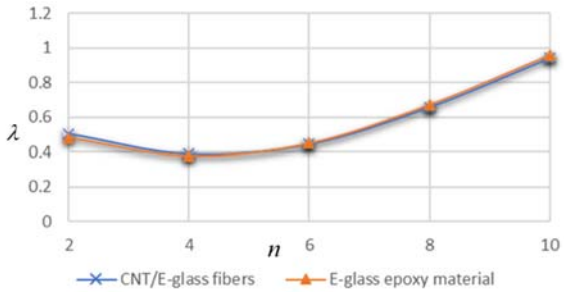

Figure 8. Frequency λ variation of 3-layered CNT-reinforced nanocomposite and without CNT composite conical shells with respect to circumferential node number n. $\alpha = 45^0, \gamma = 0.05, \beta = 0.5$.

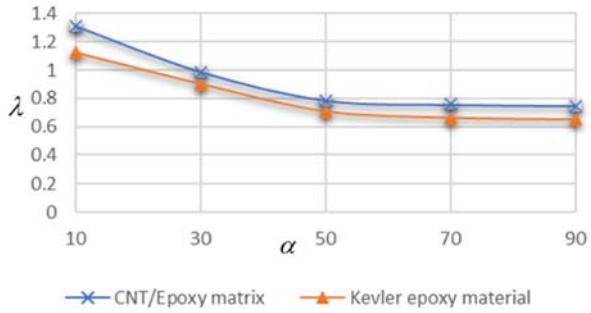

Figure 9. Frequency λ variation of 5-layered CNT-reinforced nanocomposite and without CNT composite shells varies with the cone angle α under different matrix materials. $n = 2, \gamma' = 0.5, \beta = 0.5$.

CNTs change the effective elastic moduli and density of the composite shell. Mori–Tanaka's homogenization scheme provides the effective Young's modulus, shear, and bulk moduli used in FSDT. Higher effective stiffness (for the same mass distribution), in return, produces higher natural frequencies. The volume fraction (V_f) is related to effective stiffness, so it definitely affects frequencies. An aligned CNT orientation is more effective at increasing directional stiffness (longitudinal modulus).

Figure 10 exhibits the mode shapes for the displacement function W of CNT-reinforced nanocomposite conical shells. Normalization is conducted with respect to the maximum transverse displacement W. As expected, the transverse displacements are mostly predominant.

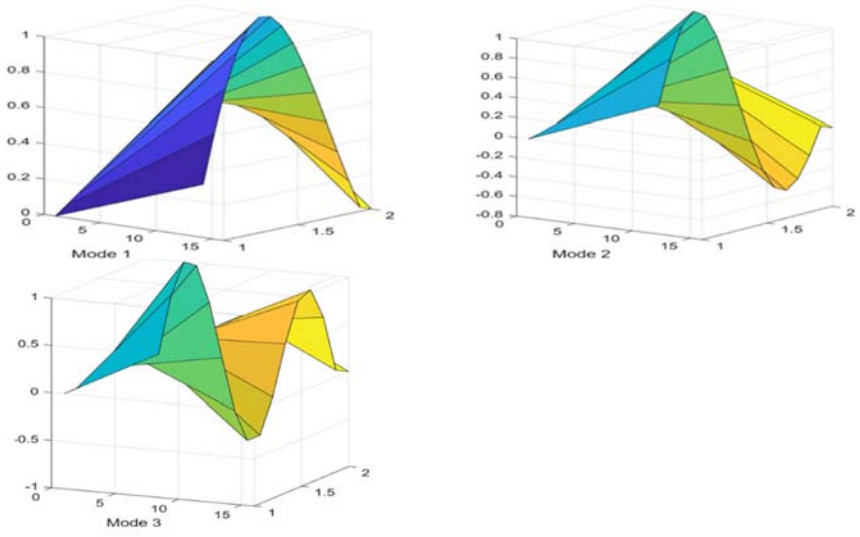

Figure 10. Mode shapes of vibration of CNT-reinforced nanocomposite conical shells. (a) Mode 1. (b) Mode 2. (c) Mode 3.

4. Conclusions

The current study presents a comprehensive analysis of the vibration behavior of CNT-reinforced nanocomposite conical shells using FSDT integrated with the Mori–Tanaka homogenization scheme. The proposed framework offers an accurate and computationally efficient approach for capturing the effects of nanoscale reinforcement on dynamic response. The incorporation of aligned CNTs within epoxy and E-glass matrices significantly improves the stiffness and damping characteristics of the composite. Macroscopic material properties are computed by the Mori–Tanaka model, considering the influence of CNT volume fraction, alignment, and dispersion.

The nondimensional angular frequency ω is extremely sensitive to the length ratio β. In all cases, increasing β from 0.1 to 0.9 results in a massive frequency increase of over 1700%. The 5-layer Kevlar/epoxy shell shows the highest sensitivity. Adding CNTs to the epoxy matrix alone actually results in a slight decrease in frequency for this specific case ($\beta = 0.5$). However, using CNTs to reinforce the E-glass fibers leads to a dramatic increase in frequency, more than doubling it to over a 100% increase. This demonstrates that the placement of the CNTs in the fibers vs. the matrix is critical. Kevlar/epoxy shells consistently have a higher natural frequency than E-glass/epoxy shells, confirming that Kevlar provides a stiffer structure. The advantage is more pronounced in the 3-ply configuration. The effect of adding more layers (from 3 to 5) is not universal and depends on the base material. For Kevlar/epoxy, the 3-ply layup is stiffer. For E-glass/epoxy, the 5-ply symmetric layup is stiffer. This highlights the complex interaction between material properties and laminate stacking sequence.

The nondimensional frequency is highly sensitive to the cone angle. In all cases, increasing the cone angle from 10° to 90° (i.e., making the shell more like a cylinder) results in a significant decrease in frequency, typically between 37% and 57%. The E-glass/epoxy shells show the greatest sensitivity to this change. The effect of CNT reinforcement is highly dependent on what it is reinforcing. Adding CNTs to the epoxy matrix results in a significant increase in frequency of around

18%. Conversely, adding CNTs to the E-glass fibers results in a large decrease in frequency of over 23%. This suggests that the effect of CNT placement is complex and interacts with the cone angle and material properties. For conical shells at this angle, E-glass/epoxy shells have a significantly higher natural frequency (over 42%) than Kevlar/epoxy shells. This is the opposite of what was observed for the length ratio in Table 5, highlighting how the optimal material depends on the geometric parameters. For conical shells, the number of layers (3 vs. 5) has a very minor effect on the natural frequency, with differences of less than 2%. The 3-ply configuration is consistently slightly stiffer, but the effect is negligible compared to the influence of material and cone angle.

The nondimensional frequency is highly sensitive to the circumferential node number. In all cases, increasing n from 2 to 10 results in a very large increase in frequency, typically between 80% and 106%. This indicates that higher-order vibration modes with more waves around the circumference have significantly higher frequencies. The 3-ply Kevlar/epoxy shell shows the greatest sensitivity. Adding CNTs provides a consistent increase in natural frequency across all material systems for this vibration mode (n = 6). The most significant benefit is seen when CNTs are used to reinforce the E-glass fibers, with an increase of over 15% for the 3-ply and a substantial 30.1% for the 5-ply layup. Reinforcing the epoxy matrix also provides a clear benefit, increasing frequency from 7.5% to 10.8%. For this specific mode (n = 6), E-glass/epoxy shells have a higher natural frequency than Kevlar/epoxy shells, with the 5-ply configuration showing a more pronounced advantage of almost 17%. This continues the trend observed with the cone angle, where E-glass outperforms Kevlar for this shell geometry. The effect of the number of layers is material-dependent. For Kevlar-based shells, the 3-ply layup is significantly stiffer (around 8%–9% with higher frequency) than the 5-ply layup. For E-glass-based shells, the difference between 3 and 5 plies is very small (<1%), with the 3-ply being marginally stiffer.

Overall, the results demonstrate that boundary conditions, ply orientation, number of layers, and shape constraints such as cone angle, length proportion, and circumferential node number substantially affect the natural frequencies. These findings can serve as a valuable reference for the manufacturing and optimization of innovative nanocomposite shell structures in aerospace, mechanical, and civil engineering applications. Numerical results demonstrate that the matrix material affects the natural frequencies. Inclusion and exclusion of CNT in composites also alter such frequencies. Moreover, the frequency value changes with the layer number. In addition to that, E-glass fibers show higher frequency values compared to the epoxy matrix.

Directions for future work: Building on the current findings, several promising directions for future work have been identified. These include the adoption of higher-order shear deformation theories, incorporation of geometric nonlinearities, exploration of thermo-mechanical effects, and development of optimization-based design strategies. Future work can incorporate CNT waviness corrections, agglomeration models, and probabilistic orientation distributions. Future models can incorporate orientation distribution functions (e.g., von Mises–Fisher ODF), randomly oriented CNT composites, and stochastic homogenization approaches to more accurately predict torsional and shear-coupled vibration responses in CNT-reinforced conical shells. Experimental validation and multiphysics extensions also represent important steps toward translating the present theoretical predictions into practical engineering applications. The insights provided by this study establish a foundation for future investigations into high-performance nanocomposite shell structures and contribute to the broader development of advanced materials for aerospace, marine, and mechanical systems.

Challenges and difficulties of the study: The investigation of the free vibration behavior of CNT-reinforced nanocomposite conical shells using FSDT and the Mori–Tanaka homogenization scheme presents several challenges. One major difficulty lies in accurately modeling the effective material properties of CNT-reinforced composites. The Mori–Tanaka approach assumes uniform dispersion and perfect interfacial bonding between CNTs and the matrix, whereas, in practice, CNTs may be unevenly distributed, misaligned, or exhibit imperfect bonding. Moreover, the conical shell geometry introduces additional complexities due to its varying curvature and thickness, which make the governing equations highly nonlinear and coupled.

Implementing FSDT further increases mathematical complexity by accounting for transverse shear effects, often requiring advanced numerical methods for solution and convergence verification. Sensitivity to parameters such as CNT volume fraction, orientation, and aspect ratio also affects the accuracy of results. Finally, experimental validation remains difficult because of limited nanoscale testing techniques and the lack of reliable benchmark data, making it challenging to confirm theoretical predictions.

Use of Generative-AI tools declaration

The author declare that she has not used Artificial Intelligence (AI) tools in the creation of this article

Acknowledgments

This work is completed by Saira Javed and is supported by Deanship of Scientific Research, Vice Presidency for Graduate Studies and Scientific Research, King Faisal University, Saudi Arabia. [Grant No.: KFU254439]

Conflict of interest

Author declares no conflicts of interest in this paper.

Reference

1. H. Afshari, H. Amirabadi, Vibration characteristics of rotating truncated conical shells reinforced with agglomerated carbon nanotubes, *J.Vib. Control*, **28** (2022), 1894–1914.
2. M. Alinejad, S. J. Mehradadi, M. M. Najafizadeh, Free vibration analysis of a sandwich conical shell with a magnetorheological elastomer core, enriched with carbone nanotubes and functionally graded porous face layers, *Noise Vib. World.*, **55** (2024), 382–406.
3. R. Bina, M. S. Tehrani, A. Ahmadi, A. G. Taki, R. Akbarian, Using 3D theory of elasticity for free vibration analysis of functionally graded laminated nanocomposite shells, *Steel Compos. Struct.*, **52** (2024), 487–499. https://doi.org/10.12989/scs.2024.52.4.487
4. K. Arshadi, M. Abasi, H. Afshari, The free vibration analysis of ring-stiffened FG conical sandwich shells with auxetic and non-auxetic honeycomb cores, *Noise Vib. World.*, **56** (2025), 76–97.

5. H. Mallek, H. Mellouli, L. B. Said, M. Wali, F. Dammak, M. Boujelbene, Bending and free vibration analyses of CNTRC shell structures considering agglomeration effects with through-the-thickness stretch, *Thin-Wall. Struct.*, **191** (2023), 111036. https://doi.org/10.1016/j.tws.2023.111036
6. J. R. Cho, Free vibration responses of functionally graded CNT-reinforced composite conical shell panels, *Polymers*, **15** (2023), 1987. https://doi.org/10.3390/polym15091987
7. H. Amirabadi, H. Afshari, M. Sarafraz, S. Rahmani, Effects of non-uniformity in thickness and volume fraction of agglomerated CNTs on the dynamics of a spinning CNT-reinforced nanocomposite truncated conical shell, *Noise Vib. World.*, **55** (2024), 167–185.
8. A. F. Fedotov, Mori-Tanaka experimental-analytical model for predicting engineering elastic moduli of composite materials, *Compos. Part B-Eng*, **232** (2022), 109635. https://doi.org/10.1016/j.compositesb.2022.109635
9. Y. A. Benveniste, A New approach to the application of Mori-Tanaka's theory in composite materials, *Mech. Mater.*, **6** (1987), 147–157. https://doi.org/10.1016/0167-6636(87)90005-6
10. P. Xiang, Q. Xia, L. Z. Jiang, L. Peng, J. W. Yan, X. Liu, Free vibration analysis of FG-CNTRC conical shell panels using the kernel particle Ritz element-free method, *Compos. Struct.*, **255** (2021), 112987. https://doi.org/10.1016/j.compstruct.2020.112987
11. Y. Zhang, W. Liu, Nonlinear vibration response of a functionally graded carbon nanotube-reinforced composite conical shell using a stress function method, *Acta Mech.*, **233** (2022), 3157–3174. https://doi.org/10.1007/s00707-022-03273-9
12. B. Thomas, T. P. Suresh, Vibration and buckling analysis of functionally graded carbon nanotube reinforced composite beams. *Int. J. Civil Eng. Technol.*, **8** (2017), 74–84.
13. N. Aghaei, M. T. Tooti, Free vibration analysis of nanotube-reinforced composite conical shell in high temperature environment, *Amirkabir J. Mech. Eng.*, **51** (2019), 101–110.
14. A. H. Sofiyev F. Tornabene, R. Dimitri, N. Kuruoglu, Buckling behavior of FG-CNT reinforced composite conical shells subjected to a combined loading, *Nanomaterials*, **10** (2020), 419. https://doi.org/10.3390/nano10030419
15. Y. Heydarpour, M. M. Aghdam, P. Malekzadeh, Free vibration analysis of rotating functionally graded carbon nanotube-reinforced composite truncated conical shells, *Compos. Struct.*, **117** (2014), 187–200. https://doi.org/10.1016/j.compstruct.2014.06.023
16. R. Ansari, J. Torabi, M. F. Shojaei, Free vibration analysis of embedded functionally graded carbon nanotube-reinforced composite conical/cylindrical shells and annular plates using a numerical approach, *J. Vib. Control*, **24** (2018), 1123–1144.
17. Y. Kiani, R. Dimitri, F. Tornabene, Free vibration study of composite conical panels reinforced with FG-CNTs, *Eng. Struct.*, **172** (2018), 472–482. https://doi.org/10.1016/j.engstruct.2018.06.006
18. F. Tornabene, E. Viola, D. J. Inman, 2-D differential quadrature solution for vibration analysis of functionally graded conical, cylindrical shell and annular plate structures, *J. Sound Vib.*, **328** (2009), 259–290. https://doi.org/10.1016/j.jsv.2009.07.031
19. M. Bulut, A numerical investigation on vibration analysis of fiber reinforced and truncated conical hollow shells with different fiber orientations, *J. Institute Sci. Technol.*, **8** (2018), 259–269.
20. M. Shadmani, A. Afsari, R. Jahedi, M. J. Kazemzadeh-Parsi, Nonlinear free vibrations analysis of truncated conical shells made of bidirectional functionally graded materials, *J. Vib. Control*, **30** (2024), 2842–2856.

21. Y. Shi, Z. Chen, D. An, J. Xu, Z. Zhou, T. Q. Bui, R. Li, New free vibration solutions of arbitrarily constrained spherical-conical shell assemblies within a state-space-based piecewise solution framework, *Thin-Wall. Struct.*, **214** (2025), 113322. https://doi.org/10.1016/j.tws.2025.113322
22. Y. Shi, D. An, J. Xu, R. Li, Traveling-wave vibration of spinning thick multi-conical shells: New solving methodology, *Int. J. Mech. Sci.*, **296** (2025), 110313. https://doi.org/10.1016/j.ijmecsci.2025.110313
23. L. L. Zhang, L. C. Zhao, S. J. Lang, K. Asemi, Free vibration analysis of functionally graded graphene platelet-reinforced metal foam doubly curved panel, *Front. Mater.*, **11** (2024), 1339865. https://doi.org/10.3389/fmats.2024.1339865
24. M. Bayat, A. Kalhori, K. Asemi, M. Babaei, Plates, beams and shells reinforced by CNTs or GPLs: A review on their structural behavior and computational methods, *Comp. Model. Eng. Sci.*, **142** (2025), 1351. https://doi.org/10.32604/cmes.2025.060222
25. F. Kiarasi, A. Asadi, M. Babaei, K. Asemi, M. Hosseini, Dynamic analysis of functionally graded carbon nanotube (FGCNT) reinforced composite beam resting on viscoelastic foundation subjected to impulsive loading, *J. Comput. Appl. Mech.*, **53** (2022), 1–23. https://doi.org/10.22059/JCAMECH.2022.339008.693
26. M. Khatoonabadi, M. Jafari, F. Kiarasi, M. Hosseini, M. Babaei, K. Asemi, Shear buckling response of FG porous annular sector plate reinforced by graphene platelet subjected to different shear loads, *J. Comput. Appl. Mech.*, **54** (2023), 68–86. https://doi.org/10.22059/JCAMECH.2023.352182.784
27. M. Babaei, F. Kiarasi, K. Asemi, Torsional buckling response of FG porous thick truncated conical shell panels reinforced by GPLs supporting on Winkler elastic foundation. *Mech. Based Des. Struc.*, **52** (2024), 3552–3581. https://doi.org/10.1080/15397734.2023.2205488
28. M. J. Bayat, A. Kalhori, M. Babaei, K. Asemi, Natural frequency characteristics of stiffened FG multilayer graphene-reinforced composite plate with circular cutout resting on elastic foundation, *Int. J. Struct. Stab. Dyn.*, **24** (2024), 2450202. https://doi.org/10.1142/S021945542450202X
29. M. Hemmatnezhad, G. Iarriccio, A. Zippo, F. Pellicano, Modal localization in vibrations of circular cylindrical shells with geometric imperfections, *Thin-Wall. Struct.*, **181** (2022), 110079. https://doi.org/10.1016/j.tws.2022.110079
30. A. Zippo, M. Barbieri, G. Iarriccio, F. Pellicano, Nonlinear vibrations of circular cylindrical shells with thermal effects: An experimental study, *Nonlinear Dyn.*, **99** (2020), 373–391. https://doi.org/10.1007/s11071-018-04753-1
31. M. Amabili, *Nonlinear vibrations and stability of shells and plates*, Cambridge University Press, 2010. https://doi.org/10.1017/CBO9780511619694
32. W. Soedel, *Vibrations of shells and plates*, 3Eds, CRC Press, 2004. https://doi.org/10.4324/9780203026304
33. A. W. Leissa, J. H. Kang, Three-dimensional vibration analysis of thick shells of revolutuion, *J. Eng. Mech.*, **125** (1999), 1365-1371. https://doi.org/10.1061/(ASCE)0733-9399(1999)125:12(1365)
34. M. Amabili, A comparison of shell theories for large-amplitude vibrations of circular cylindrical shells: Lagrangian approach, *J. Sound Vib.*, **264** (2003), 1091–1125. https://doi.org/10.1016/S0022-460X(02)01385-8

35. S. Javed, Free vibration characteristic of laminated conical shells based on higher-order shear deformation theory, *Compos. Struct.*, **204** (2018), 80–87. https://doi.org/10.1016/j.compstruct.2018.07.065
36. S. Javed, A numerical solution of symmetric angle ply plates using higher-order shear deformation theory, *Symmetry*, **15** (2023), 767. https://doi.org/10.3390/sym15030767
37. R. Ansari, E. Hasrati, J. Torabi, Nonlinear vibration response of higher-order shear deformable FG-CNTRC conical shells, *Compos. Struct.*, **222** (2019), 110906. https://doi.org/10.1016/j.compstruct.2019.110906
38. A. T. Maleki, M. Pourseifi, M. Zakeri, Effect of agglomeration of the nanotubes on the vibration frequency of the multi-scale hybrid nanocomposite conical shells: A GDQ-based study, *Waves Random Complex Media*, **32** (2022), 359–380. https://doi.org/10.1080/17455030.2020.1773007

AIMS Press